International Journal of Nanomedicine

Dovepress
open access to scientific and medical research

Open Access Full Text Article

ORIGINAL RESEARCH

Evaluation of atherosclerotic lesions using dextran- and mannan–dextran-coated USPIO: MRI analysis and pathological findings

This article was published in the following Dove Press journal:
International Journal of Nanomedicine
2 May 2012
Number of times this article has been viewed

Keiko Tsuchiya[1]
Norihisa Nitta[1]
Akinaga Sonoda[1]
Ayumi Nitta-Seko[1]
Shinichi Ohta[1]
Masashi Takahashi[1]
Kiyoshi Murata[1]
Kenichi Mukaisho[2]
Masashi Shiomi[3]
Yasuhiko Tabata[4]
Satoshi Nohara[5]

[1]Department of Radiology, [2]Department of Pathology, Shiga University of Medical Science, Otsu, Shiga, [3]Institute for Experimental Animals, Kobe University School of Medicine, Kobe, Hyogo, [4]Department of Biomaterials, Institute for Frontier Medical Sciences, Kyoto University, Kyoto, [5]Nagoya Research Laboratory, Meito Sangyo, Kiyosu, Aichi, Japan

Abstract: Magnetic resonance imaging (MRI) can detect atherosclerotic lesions containing accumulations of ultrasmall superparamagnetic iron oxides (USPIO). Positing that improved USPIO with a higher affinity for atherosclerotic plaques would yield better plaque images, we performed MRI and histologic studies to compare the uptake of dextran- and mannan–dextran-coated USPIO (D-USPIO and DM-USPIO, respectively) by the atherosclerotic walls of rabbits. We intravenously injected atherosclerotic rabbits with DM-USPIO (n = 5) or D-USPIO (n = 5). Two rabbits were the controls. The doses delivered were 0.08 (dose 1) (n = 1), 0.4 (dose 2) (n = 1), or 0.8 (dose 3) (n = 3) mmol iron/Kg. The dose 3 rabbits underwent in vivo contrast-enhanced magnetic resonance angiography (MRA) before and 5 days after USPIO administration. Afterwards, all animals were euthanized, the aortae were removed and subjected to in vitro MRI study. The signal-to-noise ratio (SNR) of the aortic wall in the same region of interest (ROI) was calculated in both in vivo and in vitro studies. Histological assessment through measurement of iron-positive regions in Prussian blue-stained specimens showed that iron-positive regions were significantly larger in rabbits injected with DM- rather than D-USPIO ($P < 0.05$) for all doses. In vivo MRA showed that the SNR-reducing effect of DM- was greater than that of D-USPIO ($P < 0.05$). With in vitro MRI scans, SNR was significantly lower in rabbits treated with dose 2 of DM-USPIO compared with D-USPIO treatment ($P < 0.05$), and it tended to be lower at dose 3 ($P < 0.1$). In conclusion, we suggest that DM-USPIO is superior to D-USPIO for the study of atherosclerotic lesions in rabbits.

Keywords: atherosclerosis, magnetic resonance imaging, contrast media, plaque, mannan–dextran-coated USPIO

Introduction

Atherosclerosis is a chronic inflammatory response to vessel wall injury, leading potentially, to acute coronary syndrome and cerebral vascular disorders, induced by plaque rupture. The noninvasive imaging of atherosclerotic plaque progression and of therapeutic response is very important. In atherosclerosis, macrophage accumulation initiates lesion development and triggers clinical events by producing several molecules that promote inflammation, plaque disruption, and subsequent thrombus formation.[1–4] However, conventional anatomic measurements of advanced lesions (eg, plaque size or luminal narrowing) do not necessarily correlate with macrophage content. It is desirable that imaging of macrophages permits the identification of highly activated plaques, to help in the prediction of acute thrombotic events, and to facilitate assessment of the therapeutic effects of antiatherosclerotic drugs, such as statins. In hyperlipidemic rabbits and humans, atherosclerotic plaques have been investigated using magnetic resonance

Correspondence: Keiko Tsuchiya
Department of Radiology, Shiga University of Medical Science, Setatsukinowa-cho, Otsu, Shiga 520-2192, Japan
Tel +81 77 548 2288
Fax +81 77 544 0986
Email keikot@belle.shiga-medac.jp

imaging (MRI), using ultrasmall superparamagnetic iron oxides (USPIO): iron oxide nanoparticles stabilized with low-molecular-weight dextran, having a mean diameter of 30 nm.[5–8] As these relatively small particles are not immediately recognized by the hepatic and splenic mononuclear phagocytic systems (MPS),[9,10] the prolongation of their intravascular half-life permits their uptake, via macrophages, by the whole body, including the lymph nodes, lungs, and the walls of atherosclerotic vessels.[5–8,11,12] With respect to the excretion pathway, USPIO particles are internalized by receptor-mediated endocytosis, and metabolized via the lysosomal pathway.[13] On internalization by macrophages, the dextran coating is progressively degraded; 89% is eliminated in urine, and the rest is excreted in feces. The iron contained in USPIO is incorporated into the body's iron store and used in hemoglobin manufacture. Like endogenous iron, it is eliminated very slowly, predominantly via the feces.[14] Based on USPIO-associated T2- and T2*-shortening effects, atherosclerotic lesions with accumulated USPIO can be detected on MRI scans. Higher doses tended to be administered in earlier animal studies. We posited that improved USPIO with higher affinity for atherosclerotic plaques would make it possible to obtain better images of plaques at lower doses.

The effectiveness of iron oxide nanoparticles, which conjugate with various biomolecules, has been studied previously in investigations of novel therapeutic actions and drug delivery, for example, in blood purification therapy and drug treatments for cancer and hyperthermia.[15–25] According to Bouhlel et al,[26] the mannose receptors of M2 macrophages are more abundantly expressed in pathological tissues of atherosclerotic lesions than in the adjacent zone. Therefore, we focused on mannan–dextran-coated USPIO (DM-USPIO), prepared in-house by adding alkali-treated mannan to dextran-coated USPIO (D-USPIO). Our working hypothesis posited that the addition of mannan to D-USPIO would facilitate its uptake by macrophage-rich atherosclerotic plaques. Here, we performed MRI and histopathological studies to compare the uptake of DM-USPIO with that of D-USPIO in atherosclerotic plaques of rabbits.

Material and methods

All experimental protocols were approved by our Animal Experimentation Committee. All experiments were conducted in accordance with the Animal Care Guidelines of Shiga University of Medical Science.

Iron oxide nanoparticles

We studied two kinds of iron oxide: DM-USPIO and D-USPIO (supplied by Meito Sangyo, Kiyosu, Aichi, Japan). Superparamagnetic iron oxide (SPIO) is a widely-used, safe, liver-specific contrast medium (Resovist®; Bayer Health Care Japan, Osaka, Japan);[27] carboxydextran covers the iron core of the iron oxide particles. The particle size of the D-USPIO used in this study is different from that of SPIO but its composition is similar. We prepared DM-USPIO by adding alkali-treated mannan to D-USPIO (Figure 1). The particle size, iron concentration, and magnetic susceptibility

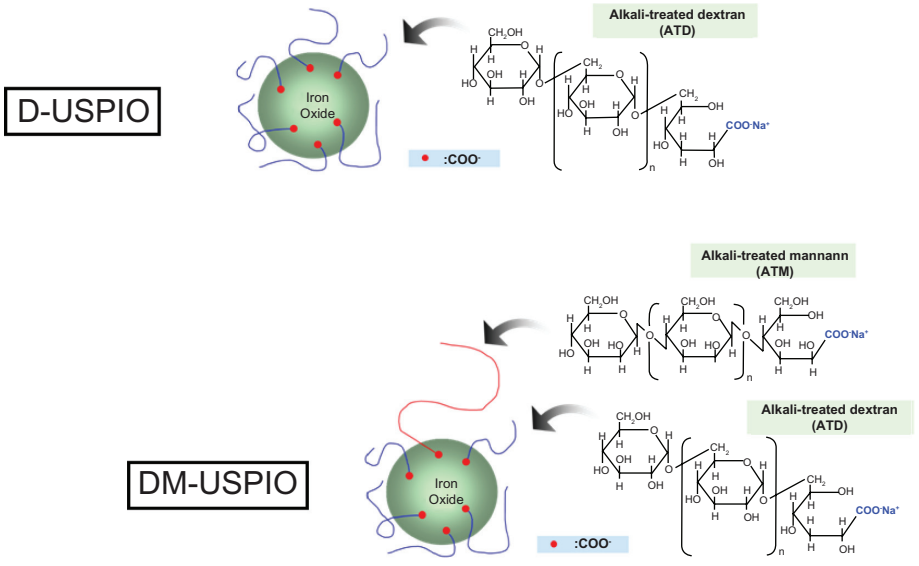

Figure 1 Illustration of D-USPIO and DM-USPIO.
Note: DM-USPIO was prepared in-house by adding alkali-treated mannan to D-USPIO.
Abbreviations: D-USPIO, dextran-coated ultrasmall superparamagnetic iron oxide; DM-USPIO, mannan–dextran-coated ultrasmall superparamagnetic iron oxide.

were the same for D- and DM-USPIO (28 nm, 15 mg/mL, 0.028 erg · gauss^{-2} · g^{-1}, respectively).

Preparation of D- and DM-USPIO

To obtain D-USPIO, 84 g of carboxydextran (molecular weight: 2500, approximately) was dissolved in 150 mL of water. To this was added an aqueous solution obtained by dissolving 17 g of ferrous chloride tetrahydrate in 130 mL of a 1 M aqueous ferric chloride solution under a nitrogen gas stream. Then, 220 mL of a 3 N aqueous solution of sodium hydroxide was added, with heating and stirring. The mixture was adjusted to pH 7.0 by adding 6 N hydrochloric acid, and then refluxed for 1.5 hours. The reaction mixture was subjected to centrifugation at 2500 × g for 1 hour, and the supernatant liquid then subjected to ultrafiltration (Centramate™; Pall Corporation, Long Island, NY) (molecular weight cut-off [MWCO]: 100,000) to obtain 1 L of D-USPIO.

To create DM-USPIO we added 500 mL of D-USPIO solution (iron concentration: 30 mg/mL) to 15 g of mannan prepared by extraction from beer yeast and refluxed for 5 hours. The reaction mixture was then subjected to ultrafiltration (MWCO: 100,000) to obtain 500 mL of DM-USPIO.

In vivo MRI

We used six Watanabe heritable hyperlipidemic (WHHL) rabbits obtained from the Institute for Experimental Animals at Kobe University, Hyogo, Japan. Each was 9–12 months old and weighed approximately 3 kg. At this age, WHHL rabbits harbor active plaque formations in the aortic wall.[28] They were divided into two equal groups and injected intravenously with 0.8 mmol iron (Fe)/kg (dose 3) of D- or DM-USPIO. Gadolinium-enhanced magnetic resonance angiography (MRA) scans were obtained before and 5 days after the injection. For each MRI session, the rabbits were fully anesthetized with ketamine (Ketalar; Daiichi Sankyo, Tokyo, Japan), at 25 mg/kg body weight, and medetomidine (Domitor; Nippon Zenyaku Kogyo, Koriyama, Fukushima, Japan), at 0.1 mg/kg body weight, then injected intravenously with 2 mL gadopentetate dimeglumine (Magnevist®; Bayer Health Care Japan), diluted in 10 mL saline.

All scans were obtained using a 1.5T MRI system, using a transmit-receive coil (Magnetom Sonata; Siemens Medical Solutions, Erlangen, Germany) (maximum amplitude: 40 mT m^{-1}; slew rate: 200 mT m^{-1} msec^{-1}). For imaging, we used a fast low-angle shot (FLASH) protocol. The parameters used were: TR, 4.3 ms; TE, 1.7 ms; flip angle, 25°; field of view (FOV), 320 × 200 mm; matrix size, 512 × 320; and slice thickness, 1 mm. The source images were made available for analysis on a workstation that allowed interactive multiplanar reformatting of the data sets.

For quantitative analysis, we calculated the signal-to-noise ratio (SNR) in the same three regions of interest (ROI) (3 × 20 pixels) in the aortic wall of the lower intrathoracic aorta in three different coronal reformatted images. We compared the SNR yielded by both types of USPIO.

In vitro MRI

Of the twelve WHHL rabbits, ten were divided into two equal groups, and injected with D- or DM-USPIO at three different doses: 0.08 (dose 1) (n = 1), 0.4 (dose 2) (n = 1), or 0.8 (dose 3) (n = 3) mmol Fe/kg. Two were untreated and served as controls. The animals were euthanized 5 days post-injection, and MRI scans of resected aortic specimens were obtained.

The specimens were placed in centrifuge tubes filled with gadopentetate dimeglumine (1:50 dilution) and 10% gelatin by weight. MRI was performed using a 1.5T MRI scanner, using a 1-channel loop coil (Signa HDxt; GE Healthcare, Little Chalfont, UK). Imaging was achieved using the three-dimensional (3D) first-spoiled GRASS protocol. The parameters used were: TR, 11.8 ms; TE, 4.1 ms; flip angle, 30°; FOV, 5 × 5 cm; matrix size, 512 × 512; slice thickness, 1 mm. Source images were made available for analysis on a workstation that enabled interactive multiplanar reformatting of the data sets.

For quantitative analysis we calculated the SNR at three ROIs (3 × 20 pixels) in the wall of the lower intrathoracic aorta in three different coronal reformatted images. We compared the results obtained after three different doses of D- and DM-USPIO.

Histological examination

Aortic specimens were fixed in 10% paraformaldehyde. From five different lesions on the lower thoracic aorta, we cut paraffin-embedded 4 μm thick sections on the axial plane. These were stained with Prussian blue to identify the accumulation of iron oxide. We also stained macrophages immunohistochemically with RAM11, and compared Prussian blue- and RAM11-stained areas. For quantitative assessment, we measured the Prussian blue-stained area in one FOV (magnification, 200×) in three different lesions for each histological section of the lower intrathoracic aorta (using Image-Pro Plus; Media Cybernetics, Silver Spring, MD), and calculated the average values. In addition, the amount of iron per unit weight (300 μg) of the lower

intrathoracic aortic specimens of dose 3 rabbits was measured by nuclear magnetic resonance (Minispec MQ20; Bruker Optics, Billerica, MA) (20 MHz, 0.47 T).

To acquire additional data on the biodistribution of D- and DM-USPIO, we examined tissues from the liver, spleen, lung, kidney, and heart of rabbits which had undergone in vivo MRI study and had received dose 3 of either D- or DM-USPIO (n = 3, respectively); two rabbits treated with neither D- nor DM-USPIO were the controls. These specimens were fixed in 10% paraformaldehyde. Paraffin-embedded 4-μm-thick sections were cut in the axial plane and stained with Prussian blue. We assessed one section for each organ. Prussian blue-stained areas were measured and evaluated as described above.

Uptake by cultured cells

To compare the phagocytosis of D- and DM-USPIO, we used the murine macrophage cell line, J774.1 (RIKEN Cell Bank; Wako, Saitama, Japan), which is widely used in research on macrophages.[29–31] Cells (8×10^5) were seeded in 12 multiwell cluster plates (Corning Inc., Corning, NY) and grown at 37°C for 24 hours in 1 mL growth medium (RPMI; Nacalai Tesque, Kyoto, Japan), supplemented with 10% bovine fetal calf serum by volume (Invitrogen, Carlsbad, CA) and 1% by weight mixed penicillin and streptomycin solution (Nacalai Tesque). The medium was then replaced with fresh medium. D-USPIO or DM-USPIO (10 μg iron oxide and 100 μL, respectively) were added, and the plates incubated for 1 hour for cell labeling. The medium was again replaced and the wells incubated for 24 hours. To identify intracellular iron oxide accumulations, the cells were stained with Prussian blue. The amount of iron contained in cell lysates was measured by atomic absorption photometry (AA-6800; Shimadzu, Kyoto, Japan). Cell labeling was performed as described in a previous study.[32]

Statistical analysis

We used SPSS for Windows software (SPSS Japan, Tokyo, Japan) for statistical analysis. Differences in the uptake of D- and DM-USPIO in the arterial wall, in the uptake of iron by cultured macrophages, and in the SNR values from MRA scans obtained in vivo and in vitro were determined using the one-tailed Student's *t*-test. A *P*-value of $P < 0.05$ was considered statistically significant.

Results

In vivo MRI

In rabbits treated with dose 3 of D- or DM-USPIO (n = 3, respectively), MRA images obtained in vivo showed irregularities, seen as spotty signal voids in the aortic wall. These were interpreted as indicating iron deposits. Before treatment with either agent, the aortic wall appeared smooth, without any evidence of atherosclerotic plaque formation. The SNR of the aortic wall was significantly lower after treatment with D- and DM-USPIO than before treatment. The difference between the SNR obtained before and after the injection of nanoparticles was significantly greater in rabbits treated with DM- rather than D-USPIO ($P < 0.05$) (Figure 2).

In vitro MRI

The aortic walls of the control animals were smooth, and the signal emitted was relatively high. In contrast, signal strength decreased in a dose-dependent fashion in rabbits injected with D- or DM-USPIO. At dose 3, the SNR tended to be lower in rabbits injected with DM- than with D-USPIO ($P < 0.1$). At dose 2 DM-USPIO, the SNRs obtained from three ROIs on three different aortic images were significantly lower than those of the rabbit treated with an equivalent dose of D-USPIO ($P < 0.05$). At dose 1, there was no statistically significant difference ($P > 0.1$) (Figure 3). These findings indicate that the uptake of either type of USPIO produced a decrease in SNR.

Histological examination

Prussian blue-stained histopathological sections showed marked iron uptake by macrophages embedded in atherosclerotic plaques in the aortic walls of rabbits injected with either type of USPIO. This was not the case in the control animals. Iron uptake was dose-dependent (Figure 4). Immunohistochemical staining (RAM11) showed that the localization of iron deposits and of macrophages coincided (Figure 5). Quantitative analysis of iron-positive areas in the aortic wall revealed that they were significantly larger in rabbits treated with dose 3 DM- than in those treated with dose 3 D-USPIO ($P < 0.05$). In addition, in different aortic sections, these areas were significantly larger in the rabbit treated with dose 1 or dose 2 DM-USPIO than in that treated with an equivalent dose of D-USPIO ($P < 0.05$) (Figure 6). At dose 3 of D- and DM-USPIO, the amount of iron accumulated per unit weight of aortic specimen was not different (Figure 7).

There was no statistically significant difference in the biodistribution of D- and DM-USPIO in tissues from the spleen and kidney. The values determined by Prussian blue staining in tissues of the spleen were 40,088 ± 10,480 vs 43,607 ± 9456 for D- and DM-USPIO, respectively, and

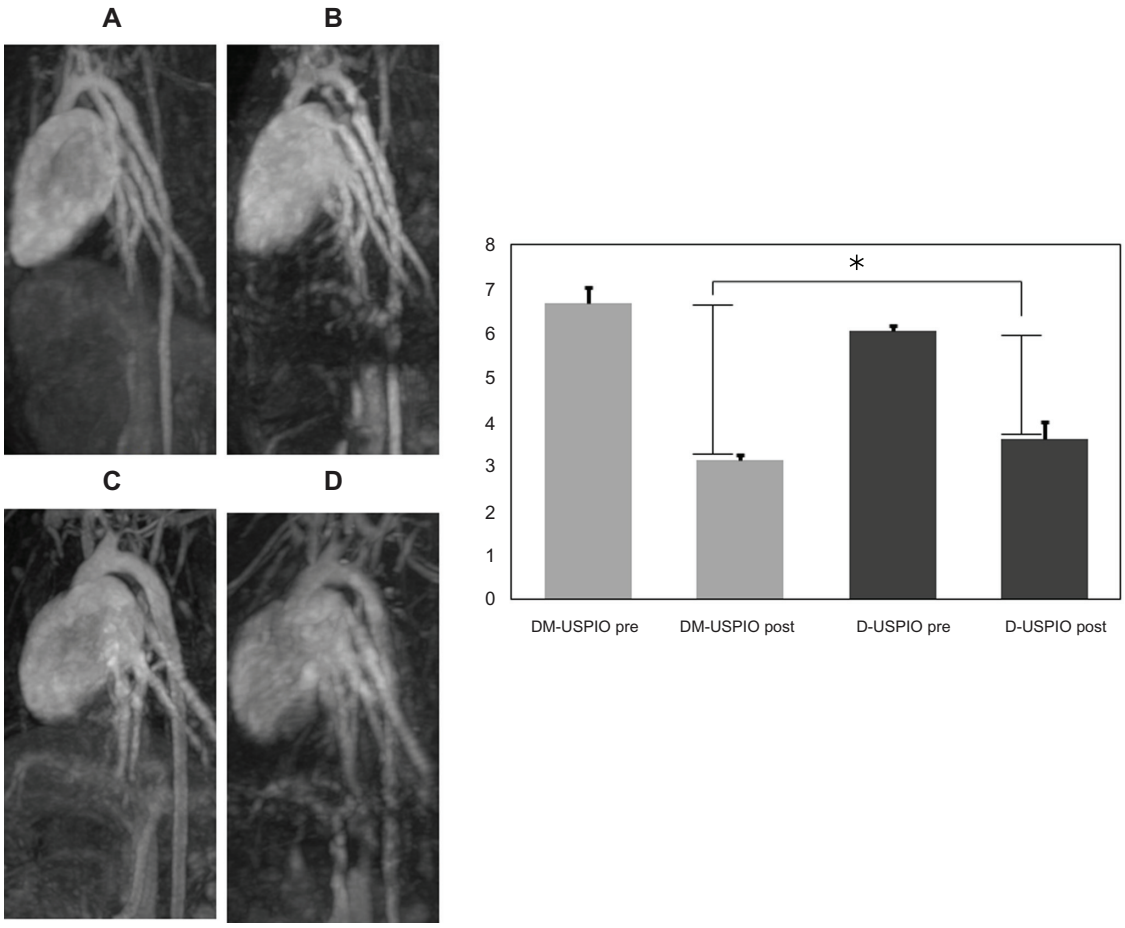

Figure 2 In vivo MRA of the thoracic aorta of WHHL rabbits, (**A**) before, and (**B**) after the administration of D-USPIO, and (**C**) before, and (**D**) after the administration of DM-USPIO.

Notes: Irregularities, seen as spotty signal voids in the aortic wall, are present on the images obtained after administration of D- or DM-USPIO. The graph compares pre- and post-administration SNR measurements in the ROI in the aortic wall of WHHL rabbits subjected to in vivo MRI (n = 6), after injection with D- or DM-USPIO (n = 3, respectively). The SNR values were significantly lower on all post-contrast images. In rabbits injected with DM-USPIO, the difference between the pre- and post-administration SNR values was significantly greater than in those treated with D-USPIO $*P < 0.05$.

Abbreviations: D-USPIO, dextran-coated ultrasmall superparamagnetic iron oxide; DM-USPIO, mannan–dextran-coated ultrasmall superparamagnetic iron oxide; MRA, magnetic resonance angiography; SNR, signal-to-noise ratio; ROI, region of interest; MRI, magnetic resonance imaging; WHHL, Watanabe heritable hyperlipidemic.

were 1711 ± 1508 vs 758 ± 583, respectively, in kidney tissues. In the liver and lung, these values tended to be higher in DM- than D-USPIO-treated rabbits (18,118 ± 5027 vs 14,421 ± 5920 in the liver, and 1261 ± 1363 vs 169 ± 245 in the lung). There was no significant iron accumulation in cardiac tissues. In the controls, only the spleen (the iron-storing organ) showed significant iron deposits. In both D- and DM-USPIO-treated rabbits these levels were increased.

Uptake by cultured cells

Microscopically, almost all cultured (J774.1) cells phagocytosed both D- and DM-USPIO. However, the amount of intracellular iron measured by atomic absorption photometry was significantly higher in cells treated with DM- rather than D-USPIO (Figure 8) ($P < 0.05$).

Discussion

Our experimental study showed that, in WHHL rabbits, both D- and DM-USPIO particles were phagocytosed by macrophages embedded in atherosclerotic plaques. This leads to a susceptibility-induced signal reduction in the atherosclerotic vessel wall on T1-weighted 3D gradient echo (GRE) images. In the T1-weighted fast 3D GRE sequence, T1 shortening is a characteristic of lower USPIO concentration. This renders the signal bright, and produces a predominant T2/T2* shortening at higher concentrations, resulting in a completely dark signal.[33] Consequently, at the initial stage of USPIO administration, the signal of the aortic lumen is completely dark due to a high blood concentration of USPIO. According to Ruehm et al,[5] the uptake by the MPS of USPIO particles over a 4- to 5-day period creates an ideal situation for imaging the vascular wall.

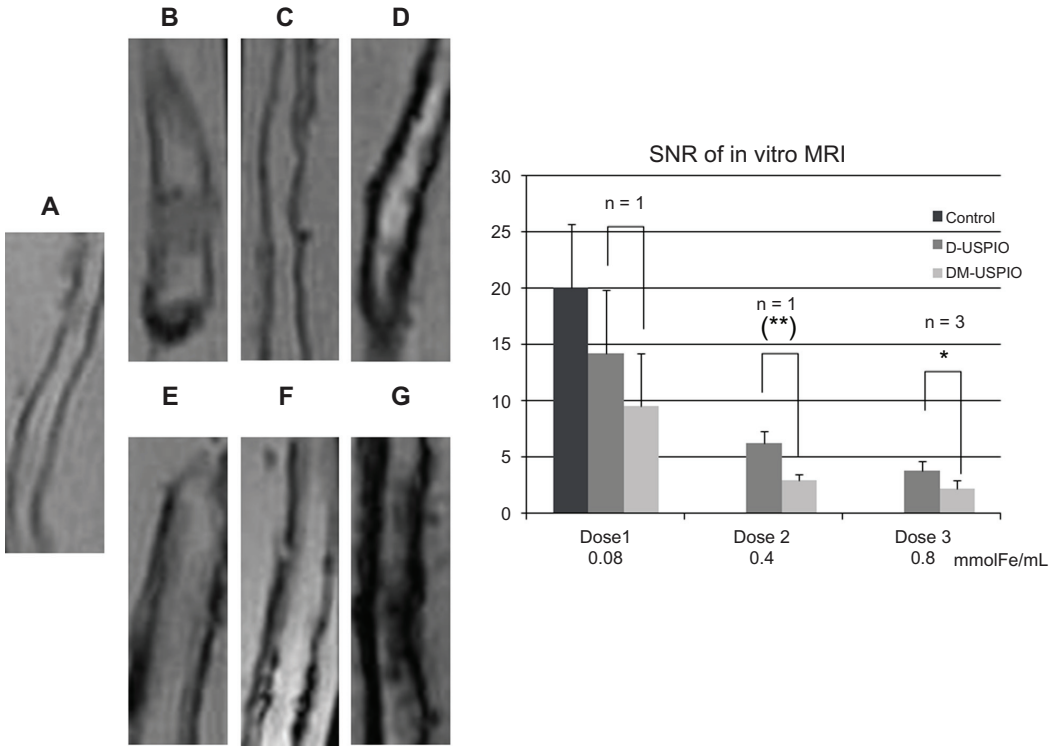

Figure 3 Graph showing the SNR of the aortic wall specimens on in vitro MRI scans.
Notes: Aortic specimens from WHHL rabbits (**A**) Controls; (**B**) dose 1, (**C**) dose 2, (**D**) dose 3 of D-USPIO; (**E**) dose 1, (**F**) dose 2, (**G**) dose 3 of DM-USPIO (dose 1: n = 1; dose 2: n = 1; dose 3: n = 3). Compared to the controls, the signal from the aortic wall decreased in rabbits injected with D- or DM-USPIO, in a dose-dependent manner. At dose 3, the SNR tended to be lower (*$P < 0.1$) in rabbits treated with DM-USPIO. The SNR value obtained from three ROIs on three different aortic images was significantly lower (**$P < 0.05$) in the rabbit treated with dose 2 DM-USPIO than in the rabbit treated with an equivalent dose of D-USPIO. There was no significant difference at dose 1 ($P > 0.1$).
Abbreviations: D-USPIO, dextran-coated ultrasmall superparamagnetic iron oxide; DM-USPIO, mannan–dextran-coated ultrasmall superparamagnetic iron oxide; SNR, signal-to-noise ratio; ROI, region of interest.

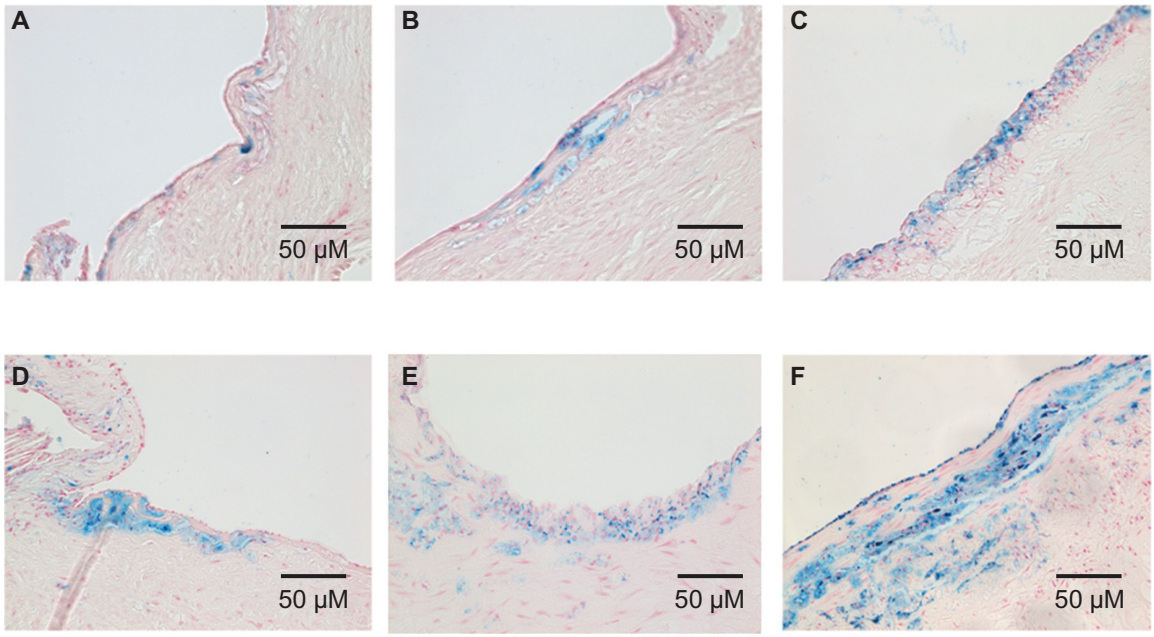

Figure 4 Prussian blue staining of histopathological sections.
Notes: (**A**) dose 1, (**B**) dose 2, (**C**) dose 3 of D-USPIO; (**D**) dose 1, (**E**) dose 2, (**F**) dose 3 of DM-USPIO. There was a marked iron uptake in the arterial walls of all rabbits injected with either D- or DM-USPIO. The Prussian blue-stained area increased in both the D- and DM-USPIO group in a dose-dependent manner.
Abbreviations: D-USPIO, dextran-coated ultrasmall superparamagnetic iron oxide; DM-USPIO, mannan–dextran-coated ultrasmall superparamagnetic iron oxide.

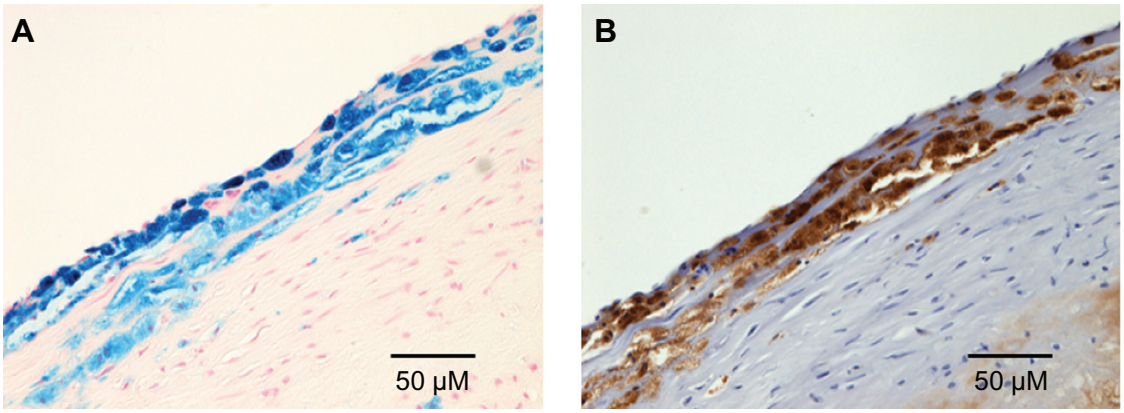

Figure 5 (**A**) Prussian blue and (**B**) immunohistochemical (RAM11) staining of histopathological sections from WHHL rabbits injected with DM-USPIO at dose 3 (0.8 mmol Fe/Kg).
Note: The localization of iron and macrophages was correlated.
Abbreviations: DM-USPIO, mannan–dextran-coated ultrasmall superparamagnetic iron oxide; WHHL, Watanabe heritable hyperlipidemic.

The iron concentration in inflammatory cells in plaques is sufficiently high for the production of dominant T2 and T2* effects, while its concentration in the blood pool is at levels at which T1 shortening effects predominate. In that study, iron particles were observed electron microscopically in actively phagocytosing cells, but not in inactive foam cells filled with fat vacuoles. These, and other observations, suggest that both D- and DM-USPIO are potential contrast agents for the diagnosis of atherosclerotic plaques – which exhibit high activity before the onset of luminal narrowing – and are potentially useful for the assessment of therapeutic effects of anti-atherosclerotic drugs, such as statins.

Macrophages and dendritic cells can be targeted by mannosylated nanoparticles because immune cells, including alveolar and peritoneal macrophages, monocyte-derived dendritic cells, and Kupffer cells, constitutively express high levels of the mannose receptor (MR). Hashida and colleagues took the lead in the development of mannosylated liposomes to target macrophages and dendritic cells for delivery (in animal models) of the anti-inflammatory agent dexamethasone

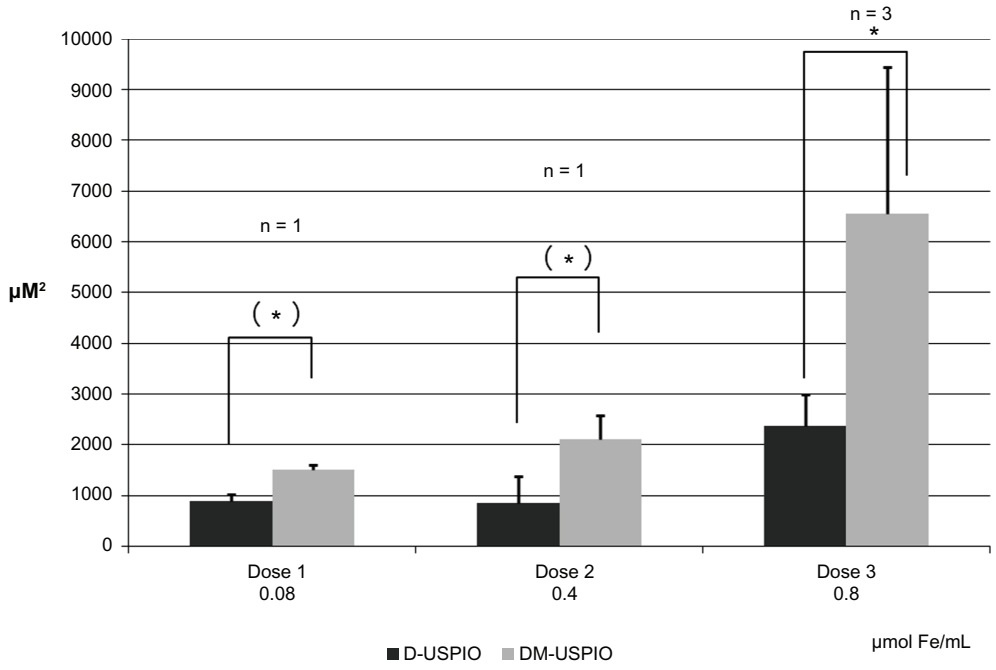

Figure 6 Iron-positive areas in the aortic wall of rabbits injected with D- or DM-USPIO.
Notes: At dose 3 (0.8 mmol Fe/Kg), the iron-positive areas were significantly larger in rabbits treated with DM- than in those treated with D-USPIO (*$P < 0.05$). The areas were significantly larger in different sections of the aorta from the rabbit injected with dose 1 or dose 2 DM- than in that treated with an equivalent dose of D-USPIO (*$P < 0.05$).
Abbreviations: D-USPIO, dextran-coated ultrasmall superparamagnetic iron oxide; DM-USPIO, mannan–dextran-coated ultrasmall superparamagnetic iron oxide.

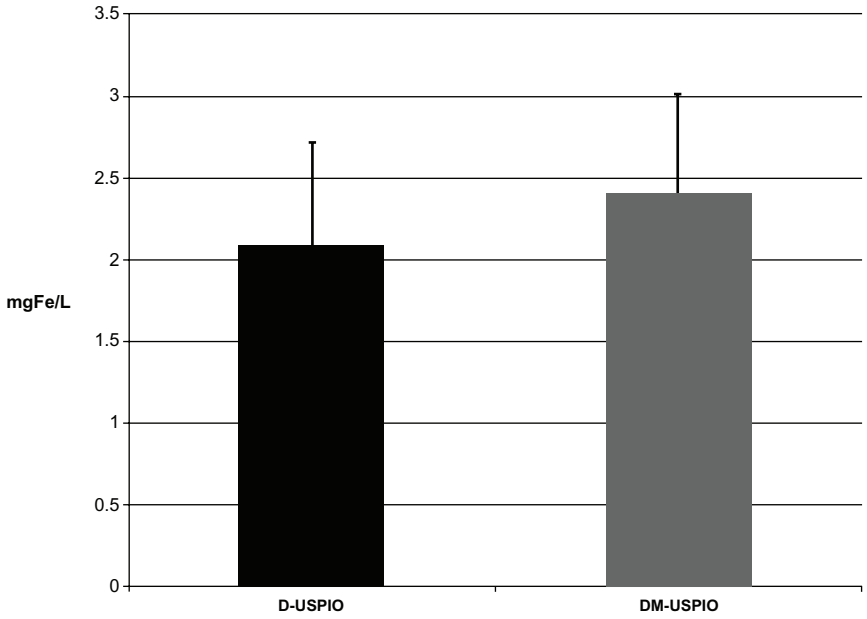

Figure 7 Iron content per unit weight of aortic specimen from rabbits injected with D- or DM-USPIO at dose 3 (0.8 mmol Fe/Kg).
Note: There was no significant difference between the two groups.
Abbreviations: D-USPIO, dextran-coated ultrasmall superparamagnetic iron oxide; DM-USPIO, mannan–dextran-coated ultrasmall superparamagnetic iron oxide.

palmitate and the CpG DNA complex.[34,35] The study showed that intratracheally administered mannosylated liposomes, with various ratios of mannosylated cholesterol derivatives, were preferentially taken up by alveolar macrophages. Inhibition studies showed that mediation occurred via mannose receptor endocytosis. Mannosylation significantly improved liposome internalization by macrophages.[36] Ross[37] identified the presence and role of activated M1 macrophages in atherosclerosis. However, the presence of M2 macrophages in atherosclerotic lesions remained unknown. Bouhlel et al[26] reported that markers of the M1 state (eg, MCP-1, IL-6, and TNF-α), and markers of M2 activation (eg, CD163, MR [also called CD206], AMAC1 [alternative macrophage activation-associated CC chemokine 1, also called chemokine ligand 18 (CCL-18)], and IL-10) are more abundantly expressed in the pathological tissues of atherosclerotic lesions than in the adjacent zone. We posit that our agent, DM-USPIO, exhibits a higher affinity for atherosclerotic lesions than does D-USPIO.

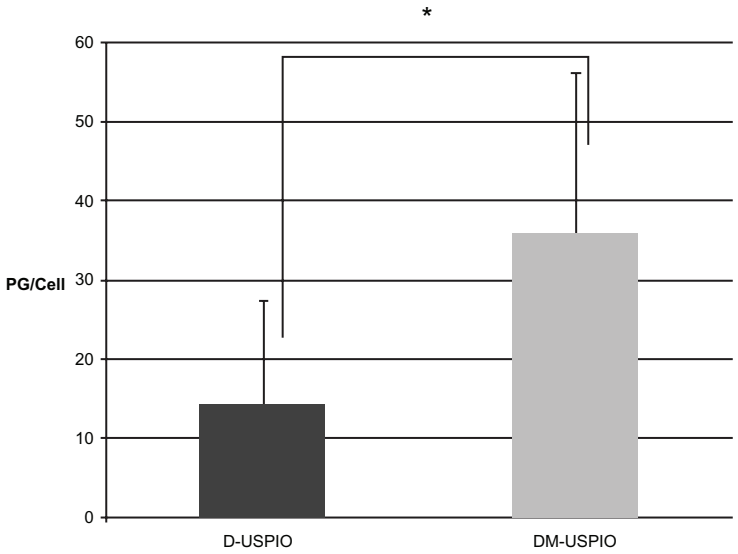

Figure 8 Iron uptake in cultured J774.1 macrophage cells, measured by atomic absorption photometry.
Note: The amount of intracellular iron was significantly higher in cells treated with DM-USPIO than with D-USPIO (*$P < 0.05$).
Abbreviations: D-USPIO, dextran-coated ultrasmall superparamagnetic iron oxide; DM-USPIO, mannan–dextran-coated ultrasmall superparamagnetic iron oxide.

Our histological analyses showed that the uptake of DM- was higher than that of D-USPIO in the atherosclerotic wall of rabbits, resulting in a greater reduction of signal from the aortic wall in MRI scans. As the amount of intracellular iron was higher in macrophage cells treated with DM- rather than D-USPIO, we posit that macrophages contained in atherosclerotic plaques are more sensitive to DM- than to D-USPIO, making it possible to acquire plaque images at lower doses of contrast agent. We also found that the distribution of DM-USPIO in the liver and lung tended to be higher than that of D-USPIO, suggesting that receptor-mediated endocytosis had a strong role in the internalization of DM-USPIO by macrophages. As mannose receptors are expressed in the liver and lung,[34–36] it is not surprising that the distribution of DM-USPIO was higher than that of D-USPIO in these organs. We cannot rule out the possibility that increased distribution in these organs results in a reduction in the amount of circulating USPIO particles, and a consequent reduction in their presence in the aortic wall. However, based on our current findings, we suggest that the affinity of DM-USPIO particles for the aortic wall affects their uptake positively, and that the effect of reduced circulation of DM-USPIO due to its distribution in the liver and lungs is not strong. This is because the circulation lifetime of USPIOs is sufficiently prolonged, in accordance with particle size. On the other hand, the amount of iron per unit weight was not different irrespective of the type of USPIO used. We attributed this to technical difficulties with our preliminary arrangements for making NMR measurements. For our NMR measurements, the uniformity of the samples was the most important issue because we used minute quantities of sample for measurement. Nevertheless, it was very difficult to obtain vessel homogenates because the vessels contained abundant fibers. Consequently, insufficient preparation of uniform homogenate samples may have impacted our NMR measurements and caused inconsistency between NMR measurements and other examinations, such as imaging and histological analysis.

Our study has some limitations. First, the number of rabbits was too small to confirm the reproducibility of the observed aortic wall changes, and assessment of inter-individual differences was not possible. Second, the USPIO doses we used were too high for clinical applications; additional studies are necessary to identify appropriate human dose levels. Also, the imaging sequence was not optimized. (The use of a more T2*-weighted GRE sequence with longer echo times may enhance the sensitivity for iron-induced susceptibility effects. With such a sequence, even smaller iron accumulations can be detected. This may facilitate a further reduction in the contrast dose). Third, after the injection of D- and DM-USPIO particles, the signal from the aortic wall was very low and not uniform among the sites examined. ROI placement affects the results of imaging analysis, and ROI analysis of the aortic wall is subject to greater dispersions. In efforts to avoid this potential bias, we used the average result from three different ROIs in our SNR measurements. Fourth, the imaging effects we observed may be specific for WHHL rabbits.

The similarity between atherosclerotic plaque formation in rabbits and humans has been documented elsewhere.[38–41] We suggest that the observed differences in the uptake of DM- and D-USPIO by rabbit atherosclerotic lesions are attributable to the binding of mannan to USPIO. Further study is required to investigate the stability of bound mannan and to determine optimum dosage amounts.

Conclusion

The trapping of DM- and D-USPIO particles in the atherosclerotic wall of rabbits was indicated by a remarkable decrease in SNR. Our histological and imaging analyses showed that DM-USPIO was taken up to a greater degree than D-USPIO. Based on our observations, we suggest that DM-USPIO is superior to D-USPIO for the study of atherosclerotic lesions.

Acknowledgments

We thank Mr Takashi Azuma (Institute for Frontier Medical Sciences, Kyoto University, Kyoto, Japan) for technical assistance with MRI scans.

Disclosure

The authors report no conflicts of interest in this work.

References

1. Aikawa M, Libby P. The vulnerable atherosclerotic plaque: pathogenesis and therapeutic approach. *Cardiovasc Pathol.* 2004;13(3):125–138.
2. Libby P, Aikawa M. Stabilization of atherosclerotic plaques: new mechanisms and clinical targets. *Nat Med.* 2002;8(11):1257–1262.
3. Shah PK. Mechanisms of plaque vulnerability and rupture. *J Am Coll Cardiol.* 2003;41(4 Suppl S):15S–22S.
4. Virmani R, Burke AP, Farb A, Kolodgie FD. Pathology of the vulnerable plaque. *J Am Coll Cardiol.* 2006;47(Suppl 8):C13–C18.
5. Ruehm SG, Corot C, Vogt P, Kolb S, Debatin JF. Magnetic resonance imaging of atherosclerotic plaque with ultrasmall superparamagnetic particles of iron oxide in hyperlipidemic rabbits. *Circulation.* 2001; 103(3):415–422.
6. Trivedi RA, Mallawarachi C, U-King-Im JM, et al. Identifying inflamed carotid plaques using in vivo USPIO-enhanced MR imaging to label plaque macrophages. *Arterioscler Thromb Vasc Biol.* 2006;26(7): 1601–1606.
7. Kooi ME, Cappendijk VC, Cleutjens KB, et al. Accumulation of ultrasmall superparamagnetic particles of iron oxide in human atherosclerotic plaques can be detected by in vivo magnetic resonance imaging. *Circulation.* 2003;107(19):2453–2458.

8. Morishige K, Kacher DF, Libby P, et al. High-resolution magnetic resonance imaging enhanced with superparamagnetic nanoparticles measures macrophage burden in atherosclerosis. *Circulation.* 2010; 122(17):1707–1715.
9. Weissleder R, Elizondo G, Wittenberg J, et al. Ultrasmall superparamagnetic iron oxide: characterization of a new class of contrast agents for MR imaging. *Radiology.* 1990;175(2):489–493.
10. Vassallo P, Matei C, Heston WD, et al. AMI-227-enhanced MR lymphography: usefulness for differentiating reactive from tumor-bearing lymph nodes. *Radiology.* 1994;193(2):501–506.
11. Weinmann HJ, Ebert W, Misselwitz B, Schmitt-Willich H. Tissue-specific MR contrast agents. *Eur J Radiol.* 2003;46(1):33–44.
12. Cho WS, Cho M, Kim SR, et al. Pulmonary toxicity and kinetic study of Cy5.5-conjugated superparamagnetic iron oxide nanoparticles by optical imaging. *Toxicol Appl Pharmacol.* 2009;239(1):106–115.
13. Schulze E, Ferrucci JT, Poss K, Lapointe L, Bogdanova A, Weissleder R. Cellular uptake and trafficking of a prototypical magnetic iron oxide label in vitro. *Invest Radiol.* 1995;30(10):604–610.
14. Weissleder R, Stark DD, Engelstad BL, et al. Superparamagnetic iron oxide: pharmacokinetics and toxicity. *AJR Am J Roentgenol.* 1989;152(1): 167–173.
15. Yung CW, Fiering J, Mueller AJ, Ingber DE. Micromagnetic-microfluidic blood cleansing device. *Lab Chip.* 2009;9(9):1171–1177.
16. Chen H, Ebner AD, Ritter JA, Kaminske MD, Rosengart AJ. Theoretical Analysis of a Magnetic Separator Device for Ex-Vivo Blood Detoxification. *Sep Sci Technol.* 2008;43(5):996–1020
17. Stamopoulos D, Benaki D, Bouziotis P, Zirogiannis PN. In vitro utilization of ferromagnetic nanoparticles in hemodialysis therapy. *Nanotechnology.* 2007;18(49):495102.
18. Stamopoulos D, Bouziotis P, Benaki D, Kotsovassilis C, Zirogiannis PN. Utilization of nanobiotechnology in haemodialysis: mock-dialysis experiments on homocysteine. *Nephrol Dial Transplant.* 2008;23(10): 3234–3239
19. Stamopoulos D, Bouziotis P, Benaki D, et al. Nanobiotechnology for the prevention of dialysis-related amyloidosis. *Ther Apher Dial.* 2009; 13(1):34–41.
20. Stamopoulos D, Manios E, Gogola V, et al. Bare and protein-conjugated Fe(3)O(4) ferromagnetic nanoparticles for utilization in magnetically assisted hemodialysis: biocompatibility with human blood cells. *Nanotechnology.* 2008;19(50):505101.
21. Yallapu MM, Othman SF, Curtis ET, Gupta BK, Jaggi M, Chauhan SC. Multi-functional magnetic nanoparticles for magnetic resonance imaging and cancer therapy. *Biomaterials.* 2011;32(7):1890–1905.
22. Thiesen B, Jordan A. Clinical applications of magnetic nanoparticles for hyperthermia. *Int J Hyperthermia.* 2008;24(6):467–474.
23. Rabias I, Tsitrouli D, Karakosta E, et al. Rapid magnetic heating treatment by highly charged maghemite nanoparticles on Wistar rats exocranial glioma tumors at microliter volume. *Biomicrofluidics.* 2010;4(2):024111.
24. Hayashi K, Ono K, Suzuki H, et al. High-frequency, magnetic-field-responsive drug release from magnetic nanoparticle/organic hybrid based on hyperthermic effect. *ACS Appl Mater Interfaces.* 2010;2(7): 1903–1911.
25. Sonoda A, Nitta N, Nitta-Seko A, et al. Complex comprised of dextran magnetite and conjugated cisplatin exhibiting selective hyperthermic and controlled-release potential. *Int J Nanomedicine.* 2010;5:499–504.
26. Bouhlel MA, Derudas B, Rigamonti E, et al. PPARgamma activation primes human monocytes into alternative M2 macrophages with anti-inflammatory properties. *Cell Metab.* 2007;6(2):137–143.
27. Kopp AF, Laniado M, Dammann F, et al. MR imaging of the liver with Resovist: safety, efficacy, and pharmacodynamic properties. *Radiology.* 1997;204(3):749–756.
28. Zimmermann-Paul GG, Quick HH, Vogt P, et al. High-resolution intravascular magnetic resonance imaging: monitoring of plaque formation in heritable hyperlipidemic rabbits. *Circulation.* 1999;99(8): 1054–1061.
29. Banerjee S, Narayanan K, Mizutani T, Makino S. Murine coronavirus replication-induced p38 mitogen-activated protein kinase activation promotes interleukin-6 production and virus replication in cultured cells. *J Virol.* 2002;76(12):5937–5948.
30. Khoury M, Escriou V, Courties G, et al. Efficient suppression of murine arthritis by combined anticytokine small interfering RNA lipoplexes. *Arthritis Rheum.* 2008;58(8):2356–2367.
31. Taniguchi S, Yanase T, Kobayashi K, Takayanagi R, Nawata H. Dehydroepiandrosterone markedly inhibits the accumulation of cholesteryl ester in mouse macrophage J774-1 cells. *Atherosclerosis.* 1996;126(1):143–154.
32. Jo J, Aoki I, Tabata Y. Design of iron oxide nanoparticles with different sizes and surface charges for simple and efficient labeling of mesenchymal stem cells. *J Control Release.* 2010;142(3):465–473.
33. Rozneman Y, Zou XM, Kantor HL. Signal loss induced by superparamagnetic iron oxide particles in NMR spin-echo images: the role of diffusion. *Magn Reson Med.* 1990;14(1):31–39.
34. Wijagkanalan W, Higuchi Y, Kawakami S, et al. Enhanced anti-inflammation of inhaled dexamethasone palmitate using mannosylated liposomes in an endotoxin-induced lung inflammation model. *Mol Pharmacol.* 2008;74(5):1183–1192.
35. Kuramoto Y, Kawakami S, Zhou S, et al. Use of mannosylated cationic liposomes/immunostimulatory CpG DNA complex for effective inhibition of peritoneal dissemination in mice. *J Gene Med.* 2008;10(4): 392–399.
36. Wijagkanalan W, Kawakami S, Takenaga M, et al. Efficient targeting to alveolar macrophages by intratracheal administration of mannosylated liposomes in rats. *J Control Release.* 2008;125(2):121–130.
37. Ross R. Atherosclerosis is an inflammatory disease. *Am Heart J.* 1999; 138(5 Pt 2):S419–S420.
38. Esper E, Chan EK, Buchwald H. Natural history of atherosclerosis and hyperlipidemia in heterozygous WHHL (WHHL-Hh) rabbits. I. The effects of aging and gender on plasma lipids and lipoproteins. *J Lab Clin Med.* 1993;121(1):97–102.
39. Esper E, Runge WJ, Gunther R, Buchwald H. Natural history of atherosclerosis and hyperlipidemia in heterozygous WHHL (WHHL-Hh) rabbits. II. Morphologic evaluation of spontaneously occurring aortic and coronary lesions. *J Lab Clin Med.* 1993;121(1):103–110.
40. Donnelly TM, Kelsey SF, Levine DM, Parker TS. Control of variance in experimental studies of hyperlipidemia using the WHHL rabbit. *J Lipid Res.* 1991;32(7):1089–1098.
41. Atkinson JB, Hoover RL, Berry KK, Swift LL. Cholesterol-fed heterozygous Watanabe heritable hyperlipidemic rabbits: A new model for atherosclerosis. *Atherosclerosis.* 1989;78(2–3):123–136.